Improvement in the Thermostability of a β-Amino Acid Converting ω-Transaminase by Using FoldX

Oliver Buß,[b] Delphine Muller,[b] Sven Jager,[c] Jens Rudat,[b] and Kersten S. Rabe*[a]

ω-Transaminases (ω-TAs) are important biocatalysts for the synthesis of active, chiral pharmaceutical ingredients containing amino groups, such as β-amino acids, which are important in peptidomimetics and as building blocks for drugs. However, the application of ω-TAs is limited by the availability and stability of enzymes with high conversion rates. One strategy for the synthesis and optical resolution of β-phenylalanine and other important aromatic β-amino acids is biotransformation by utilizing an ω-transaminase from *Variovorax paradoxus*. We designed variants of this ω-TA to gain higher process stability on the basis of predictions calculated by using the FoldX software. We herein report the first thermostabilization of a nonthermostable *S*-selective ω-TA by FoldX-guided site-directed mutagenesis. The melting point (T_m) of our best-performing mutant was increased to 59.3 °C, an increase of 4.0 °C relative to the T_m value of the wild-type enzyme, whereas the mutant fully retained its specific activity.

Introduction

The amination of ketone substrates is an important and well-known enzymatic process involved in the metabolism of all organisms. This conversion is often catalyzed by pyridoxal-5-phosphate (PLP)-dependent transaminases, which mediate the transfer of an amino group from a donor substrate to an acceptor substrate. This reaction is mechanistically split into two half-reactions and can be described by a ping-pong bi–bi mechanism that converts two substrates into two products.[1] The first part of this reaction mechanism leads to a reaction between the aldehyde group of the cofactor PLP and the ε-amine of the catalytically active lysine. The bound cofactor also helps to stabilize and to maintain the activity of the enzyme during longer incubations (Scheme 1).[2]

This highly reactive imine bond between the cofactor and ε-amino group of the lysine residue can be easily hydrolyzed to release PLP, which reacts with an amino donor molecule in the active site (Scheme 1, steps F to A). This mechanism was initially described in detail by Kirsch et al.[3] The PLP–amino donor complex in turn is also hydrolyzed, and the corresponding deaminated molecule is released. A mechanistically important lysine helps to deprotonate the amino donor–cofactor intermediate for the formation of the ketone, aldehyde, or keto acid (Scheme 1, steps C to D).[4] In the second part of the reaction mechanism, aminated PLP, pyridoxamine phosphate (PMP), reacts with an acceptor molecule, such as a keto acid, aldehyde, or ketone, to generate PLP and the corresponding amine/amino acid, which is released.[4,5] If no competing substrate is located in the active site of the enzyme, free PLP can be bound again by the ε-amino group of catalytically active lysine; this results in the initial state of the enzyme, and thus, another round of catalysis can occur. Binding of the cofactor to the enzyme leads to light absorption in the visual range, and this results in a yellow appearance of the enzyme. This complex allows direct quantification of the active ω-transaminase (ω-TA) in solution.[2] The reaction is catalyzed by ubiquitous α-transaminases and leads to α-amino acids such as L-glutamate and L-aspartate, a reaction known for almost all organisms.[6,7] However, transaminases do not only synthesize α-amino acids, they also act on molecules without ketone functions in non-α-positions or even without any carboxylic group.[8] These ω-TAs can also be classified as amine transaminases, especially if they show activity towards amines without carboxylic groups.[9] In this paper, all enzymes with amino transferase activity are classified as ω-TAs. The properties to accept non-α-keto acids make ω-TAs desirable enzymes, as this enables the synthesis of a wide spectrum of chiral amines and amino acids from prochiral substrates with predefined stereochemistry depending on the use of either an *R*- or *S*-selective enzyme.[10] This difference in enantiopreference is accompanied by a different protein fold, known as fold type IV (*R*) and I (*S*) of the PLP-dependent enzymes.[5,11] The acceptor molecules can vary from classical α-keto acids to β-, γ-, or ε-keto acids, and even ketones and alde-

[a] *Dr. K. S. Rabe*
Institute for Biological Interfaces I, Karlsruhe Institute of Technology (KIT)
Hermann-von-Helmholtz-Platz 1
76344 Eggenstein-Leopoldshafen (Germany)
E-mail: kersten.rabe@kit.edu

[b] *O. Buß, D. Muller, Dr. J. Rudat*
Institute of Process Engineering in Life Sciences, Section II: Technical Biology
Karlsruhe Institute of Technology (KIT)
Engler-Bunte-Ring 3, 76131 Karlsruhe (Germany)

[c] *S. Jager*
Computational Biology, Technische Universität Darmstadt
Schnittspahnstrasse 2, 64287 Darmstadt (Germany)

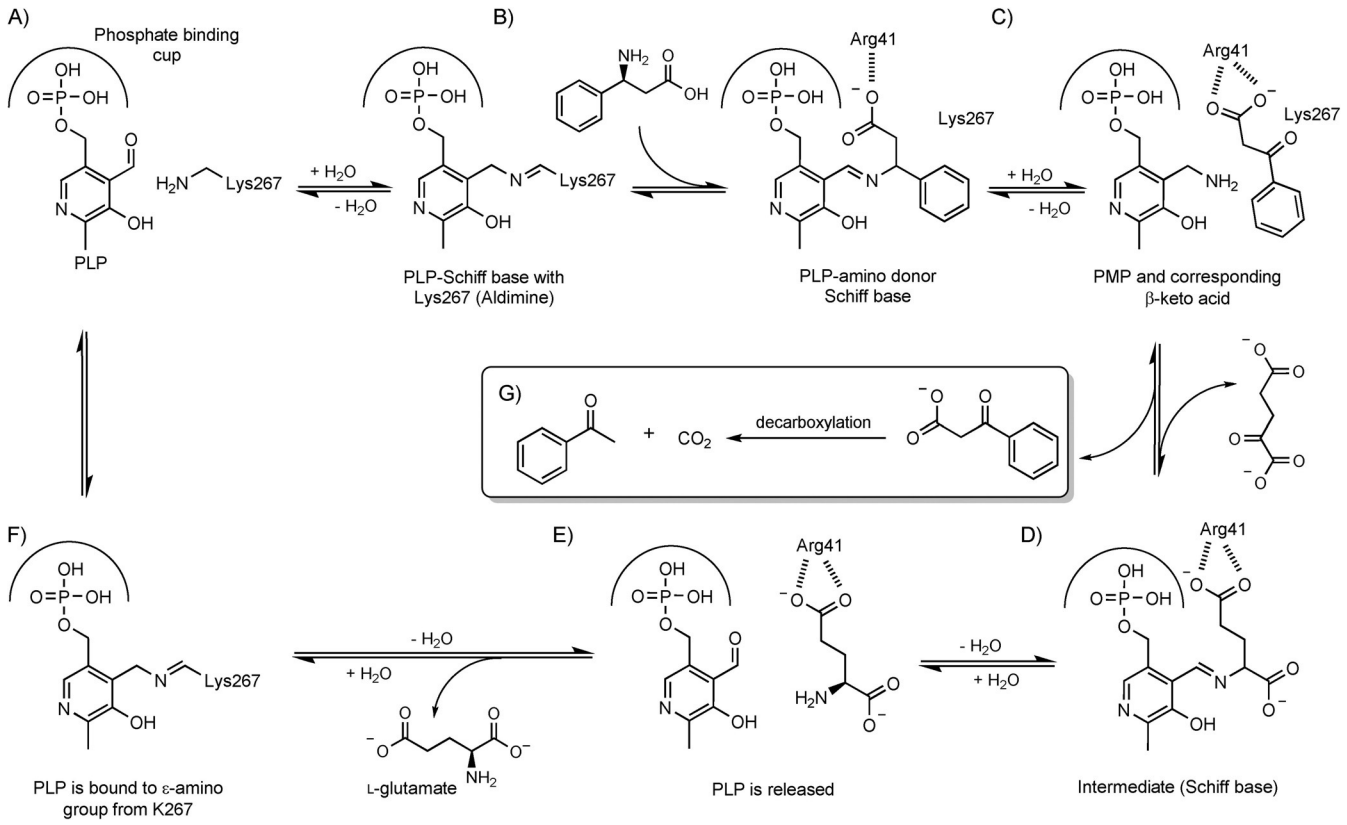

Scheme 1. ω TA catalyzed reaction mechanism with β phenylalanine as an amino donor and α ketoglutarate as an acceptor. The corresponding β keto acid of β PA spontaneously decarboxylates to acetophenone and carbon dioxide. The residues Lys267 and the carboxyl group coordinating Arg41 are labeled according to the sequence of *V. paradoxus*. Furthermore, the highly conserved phosphate binding cup is indicated. Modified after Elliot et al.[4]

hydes are converted by this class of enzymes.[12–14] Recently, ω-TAs have gained attention as important biocatalysts for the synthesis of pharmaceuticals, including the drugs sitagliptin and imagabalin.[15,16] They were intensively reviewed by Guo et al. and Dold et al., and the importance of ω-TAs for industrial applications was shown by Fuchs et al.[14,17,18]

Engineering of ω-TAs

Although there is an increasing number of ω-TAs being described, certain limitations concerning the substrate scope and physicochemical properties such as stability are still hampering their application. The pool of *R*-selective ω-TAs is still much smaller than that of *S*-selective ω-TAs, and specifically, more bulky substrates are still challenging. To overcome the latter limitation, the pharmaceutical companies Merck and Codexis performed a sophisticated directed evolution of an *R*-selective ω-TA to gain an enzyme with activity towards the substrate prositagliptin. In this process, the activity, solvent stability, and thermostability were improved by several rounds of random and site-directed mutagenesis experiments.[15] In total, 27 mutations were introduced into the ω-TA, which originated from *Arthrobacter sp.* KNK 168. There are other examples for the redesign of *S*-selective ω-TAs by Midelfort et al. and Pavlidis et al.[16,19] Midelfort et al. redesigned an *S*-selective ω-TA from *Vibrio fluvialis* towards higher activity to the aliphatic β-keto ester substrate ethyl 5-methyl 3-oxooctanoate and towards higher stability in organic solvents. Apart from this, many more examples have been described, such as examples concerning the engineering of a ω-TA regarding the promiscuity and selectivity of these enzymes.[20–25]

Thermostability

Apart from engineering the substrate scope, improving the stability of an enzyme can lead to more efficient production processes and enable the enzyme to tolerate more mutations in general. Deepankumar et al. showed the incorporation of the noncanonical α-amino acid fluorotyrosine in an *S*-selective ω-TA from *Vibrio fluvialis*. The resulting enzyme showed an increase in thermostability that was approximately 2.3-fold higher than that of the wild type. The experiments were performed at an incubation temperature of 50 °C, and the authors observed an improved half-life time of 7.0 h in comparison to 3.0 h for the wild-type enzyme. However, the melting temperature was not reported.[26] Pannuri et al. utilized five cycles of error-prone PCR and screening, which resulted in an enzyme, based on an *S*-selective ω-TA (CNB05-01) from *Arthrobacter citreus*, with improved stability. This was mainly due to important exchange of a cysteine residue to a tyrosine residue located near the active site. The optimum reaction temperature (T_{opt}) was enhanced from 30 to 55 °C and the activity was increased

approximately 260-fold, without compromising the enantioselectivity.[20,27] A rational thermostabilization strategy was recently shown for the fold type IV *R*-selective ω-TA from *Aspergillus terreus* by calculation of $\Delta\Delta G^{fold}$, combined with the crystallography B-factor set as a prefilter for $\Delta\Delta G^{fold}$ calculations, which resulted in a 2.2-fold improvement in the half-life at 40 °C with a single mutation.[28]

Apart from engineering ω-TAs from mesophilic sources, thermostable variants can, in general, also be established by screening enzymes from thermophilic organisms. The first *S*-selective ω-TA that was labeled as thermostable was discovered by an in silico screening in the thermophilic microorganism *Sphaerobacter thermophilus*. This enzyme showed remarkable stability and retained its full activity at 60 °C for at least 2 h.[12] The same research group identified and characterized a thermostable ω-TA with activity towards amines by using a modified NCBI-blast search in the thermophilic microorganism *Thermomicrobium roseum*. This enzyme showed a melting point (T_m) of 87 °C.[29] The ω-TA lost only half of its initial activity after incubating at 60 °C for 12.5 h. Ferrandi et al. discovered three thermostable ω-TAs from hot-spring metagenomes, and the best was a ω-TA from an unknown microorganism, labeled as B3-TA, with a T_m of 88 °C.[30] This enzyme was found to be very robust and showed long-term stability at 80 °C for at least 2 weeks; it lost only 60% of its initial activity under these conditions. The other two enzymes, Is3 and It6, showed T_m values of 79 and 57 °C, respectively.

In summary, up to now only five *S*-selective ω-TAs have been described to exhibit high thermostability, and only one of these ω-TAs from *Sphaerobacter thermophiles* shows activity towards *rac*-β-phenylalanine (β-PA). β-PA is an important aromatic β-amino acid that is also part of the antitumor agent paclitaxel and the antitumor antibiotic C-1027.[31,32] Besides this, β-PA and derivatives thereof can also be utilized in β-peptides, as inhibitor for peptidase IV and in drug-delivery systems.[33–35] The β-PA-converting ω-TA from *S. thermophiles* shows only a low activity of 3.3 U mg^{-1} compared to the ω-TA from *Variovorax paradoxus* with a specific activity of 17.5 U mg^{-1} at 37 °C.[36] Thus, the transaminase from *V. paradoxus* is an interesting candidate for enzyme engineering taking into account its high enzymatic activity and lack of data concerning thermostabilization.

The aim of this study was to optimize the thermostability of the *V. paradoxus* transaminase (ω-VpTA) by using an in silico approach in combination with site-directed mutagenesis to generate an enzyme with a longer lifetime at temperatures above 50 °C. The FoldX software was utilized to identify potentially stabilizing mutations to reduce necessary sample throughput and to avoid large enzyme libraries and the corresponding need for a high-throughput screen.[37] FoldX can be used to calculate the change in free energy caused by substitution of an amino acid and to predict the change in the free energy to fold/unfold ($\Delta\Delta G$) a protein.[37] We sequentially exchanged every amino-acid position in ω-VpTA against any standard α-amino acid and performed the free-energy calculations. The hits with the highest beneficial energy stabilization were selected for site-directed mutagenesis. Variants with high activity in cell lysate were purified and characterized in detail with regard to their thermostability and specific activity. Furthermore, the long-term activity was studied and compared to that of the wild-type enzyme.

Results and Discussion

The improvement in the thermostability of the ω-VpTA was performed by using FoldX-guided site-directed mutagenesis and was subsequently analyzed by determining the melting temperature of the resulting proteins and following their reaction with *rac*-β-PA and α-ketoglutaric acid as substrates at different temperatures. After calculating $\Delta\Delta G$ values for all 8246 possible single-site mutations, we selected the 11 most-stabilizing mutations with $\Delta\Delta G$ values ranging from 30.1 to 54.3 kcal mol^{-1}. Interestingly, the FoldX algorithm suggested to mutate glycine into much larger residues in 4 out of these 11 cases at positions 165, 325, 420, and 98. Many of the suggested mutation sites can be found at the surface of the enzyme and at a distance of more than 20 Å from the center of the enzyme, defined by the active-site lysine (K267, see also Scheme 1) binding the cofactor (Table 1 and Figure 1). However, three suggested mutation sites were closer to the active site (G165, S395, M243) with M243 in a very close proximity of only 5.0 Å to K267.

Table 1. Mutation sites with the most negative $\Delta\Delta G$ values as predicted by FoldX. The last two mutations (M243 and T408) were selected because they showed predicted stabilization with a high energy benefit in parts of the whole energy equation. The distances to the active site lysine binding the cofactor (K267, Scheme 1) were calculated by using Chimera 1.1.[53]

Position	Original amino acid	Best amino acid mutation	$\Delta\Delta G$ [kcal mol^{-1}]	Distance to K267 [Å]
165	G	M	54.3	13.5
391	E	K	42.9	24.5
325	G	D	35.9	20.4
420	G	E	35.5	26.5
19	D	M	34.6	29.3
98	G	M	34.2	29.1
345	E	F	33.5	31.2
392	D	K	30.9	21.5
395	S	I	30.1	13.2
408	T	D	11.7	21.2
243	M	R	9.5	5.0

The variants were generated in a codon-optimized ω-VpTA gene by using touch-down PCR with mismatch primers and were expressed in *Escherichia coli* BL21. To reduce the number of proteins that had to be purified, the enzymatic activity was preliminarily checked in the lysate of small expression cultures. M243R, G325D, and G420E showed no or low activity in the lysate towards (*S*)-β-PA and were thus excluded from further studies. M243R might be too close to the catalytically active lysine and also introduces a positive charge into the substrate pocket.

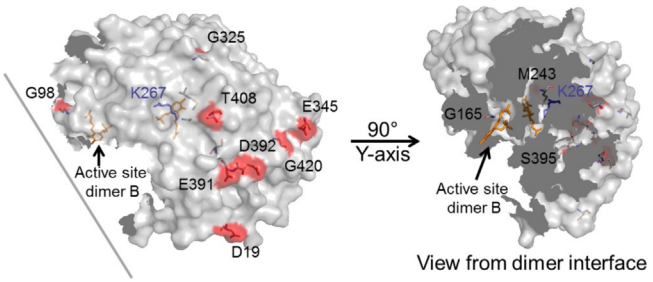

Figure 1. Locations of the 11 mutations predicted to be most stabilizing. Only one monomer of the dimeric *V. paradoxus* ω TA (chain A) is shown (PDB ID: 4AOA).[36] Note that the interface area is about one quarter of the whole protein surface (4400 Å^2). The solvent accessible parts of the mutation sites are colored in red, and the two active sites are visualized by 4′ deoxy 4′ acetylyaminopyridoxal 5′ phosphate from the crystal structure (orange). The active site lysine K267 (see also Scheme 1) is colored in blue.

All of the other hexahistidine-tagged proteins were expressed and purified by using immobilized metal-ion affinity chromatography (IMAC). Variants with low protein yield in *E. coli* BL21 resulted in a low grade of purity and were also excluded. The purity was judged on the basis of SDS-PAGE analysis of two independent protein expression and purification experiments. The ratio of the variant proteins versus other protein impurities was too high to determine the melting temperatures in those cases. An average T_m value was calculated on the basis of the data determined by using a thermal shift assay with SYPRO-orange as the protein-binding fluorescence dye in a classical qPCR-cycler system (Table 2). Of the five enzyme variants analyzed, the G98M mutation showed the highest increase in T_m of $+4\,^{\circ}C$ in comparison to the wild-type enzyme. The mutations at E345F and D392K also showed increases in the T_m value of $+0.9\,^{\circ}C$ and $+1.4\,^{\circ}C$, respectively. However, the experimental error in these cases was in the same range as the change, as can be seen upon comparing the experimental T_m and theoretical $\Delta\Delta G$ values in Table 2. Additionally, we combined the second- and third-best variants with G98M to gain an additional increase in T_m. However, no significant improvement could be achieved, which also suggested that the improvement for the single-site variants was not significant. To analyze the effect of the mutations on the specific enzyme activity, all selected variants were compared to the wild-type enzyme (Table 2).

Table 2. Experimental thermostability analysis of FoldX predicted ω VpTA variants. The measurements were conducted in triplicate and expression of every variant was performed twice (SD = standard deviation). $\Delta\Delta G$ values from Table 1 are included for comparison.

Variant	Location	$T_m \pm$ SD [°C]	ΔT_m [°C]	$\Delta\Delta G$ [kcal mol^{-1}]
G165M	loop (active site)	56.0 ± 0.2	+0.7	54.3
E391K	loop (surface)	54.3 ± 0.1	1.0	42.9
G98M	α helix (interface)	59.3 ± 0.7	+4.0	34.2
E345F	α helix (surface)	56.2 ± 1.0	+0.9	33.5
D392K	loop (surface)	56.7 ± 1.0	+1.4	30.9
G98M + E345F		58.8 ± 0.5	+3.5	
G98M + D392K		59.4 ± 0.7	+4.1	
wild type		55.3 ± 0.2	0	

To analyze whether the mutations introduced compromised the specific activity of the mutant enzymes, the reaction catalyzed by all variants was analyzed (Figure 2). The reactions were performed out at 40 °C with 15 mM *rac*-β-PA and 15 mM of the amino-acceptor substrate α-ketoglutarate, which was shown to be the best substrate for the *S*-selective ω-TA from *V. paradoxus*.[36]

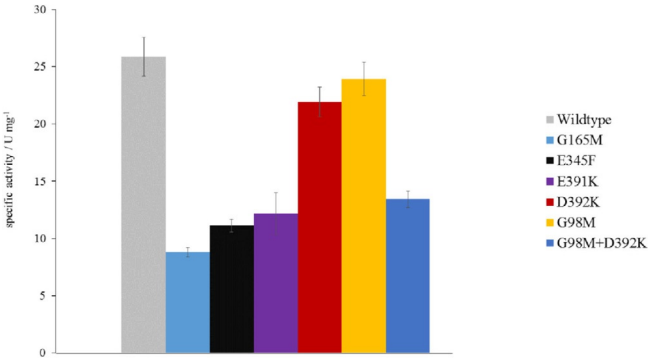

Figure 2. Comparison of specific enzyme activity of selected mutant variants against wild type ω TA. The reaction mixture contained 15 mM *rac* β PA and 15 mM α ketoglutarate. The activity was measured at 40 °C in 40 mM sodium phosphate buffer (pH 7.2). Samples were analyzed after 15 and 90 s by HPLC with precolumn derivatization.

The specific activity of the wild-type ω-TA under these conditions was determined to be 26 U mg^{-1}, which fits well with the results of Crismaru et al.[36] They determined a specific activity of 17.5 U mg^{-1} at 30 °C and 33 U mg^{-1} at 50 °C for the conversion β-phenylalanine. Our most thermostable variant, G98M, showed a slightly lower specific activity of 24 U mg^{-1}, followed by D392K with 22 U mg^{-1}. All other variants were clearly less active than the wild-type enzyme. The mutation G165M showed the lowest activity, possibly as a result of the relative close proximity of the active site (Table 1). On the basis of these results, the variants G98M and D392K and their combination were selected for further investigations regarding heat stability and were compared to the wild-type enzyme (Figure 3). The enzymes were incubated at defined temperatures (50, 55, 60, and 65 °C) in buffer solution for 20 min. After incubation, samples of the variants were retrieved, and the activities were determined at 40 °C with *rac*-β-PA as the substrate.

In accordance with the data from the determination of T_m (Table 2), the preincubation activity test showed that the wild-type enzyme rapidly lost activity at temperatures above 55 °C. However, at this temperature the variant G98M and the double-mutant G98M D392K retained relative enzymatic activities of 62 and 70% respectively, as reflected by the higher T_m values of 59.3 and 59.4 °C. The single-mutation D392K showed behavior comparable to that of the wild-type. At 65 °C, no variant showed any significant remaining activity, which is in agreement with the T_m experiments. As 55 °C was described as the optimum temperature for ω-VpTA, the long-term stability

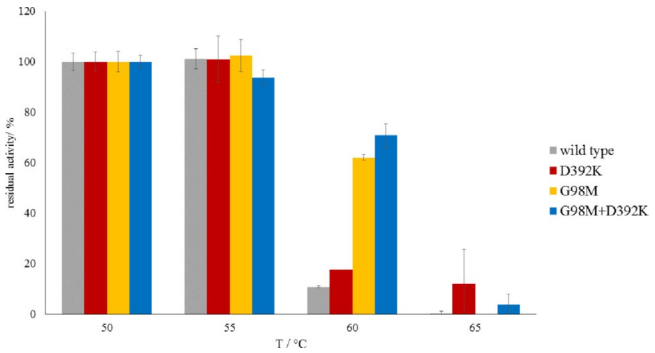

Figure 3. Enzyme activity of the best ω TA variants and the wild type after preincubation at 50, 55, 60, and 65 °C. 4 μM of the purified enzyme variants was preincubated for 20 min and was subsequently employed to convert *rac* β PA at 40 °C. Note that for the values at 65 °C, the error bars were higher than the activity determined; thus, the variants were considered in active at this temperature.

of the wild-type and our best mutant, G98M, at this incubation temperature was investigated (Figure 4).[36] Whereas after 30 min at this temperature the remaining activity of the wild-type enzyme was only 20%, our best variant, G98M, retained 80% of its activity for 30 min and still showed approximately 50% of the initial activity after incubating for 1.5 h.

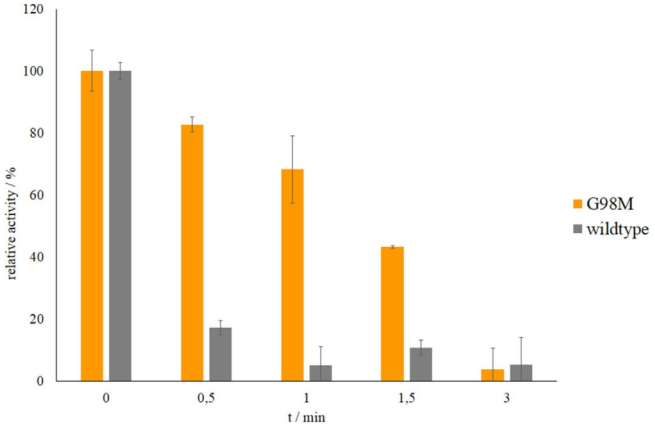

Figure 4. Long term stability of ω VpTA wild type and G98M upon incubation at 55 °C. The reaction was performed with 15 mM *rac* β PA and 15 mM α ketoglutarate as substrates at 40 °C. 4 μM of the enzyme solution was incubated in a PCR cycler to prevent condensation of water at the lid and was incubated in 40 mM sodium phosphate at pH 7.2 for a defined time.

The quite long retention of activity over time shows that the mutation site G98M is very beneficial for the stability of the enzyme. The improvement in $\Delta\Delta G$ calculated on the basis of the T_m measurements was approximately 15 kcal mol^{-1} with a ΔT_m value of 4 °C.[38] This would allow reactions at 55 °C with higher total turnovers of β-PA without a decrease in optimal catalytic activity. By contrast, the only known thermostable β-PA-converting ω-TA from *S. thermophiles* shows higher stability up to even 60 °C but more than 80% lower activity of 3.3 U mg^{-1} at 37 °C, and no absolute activity was given for 60 °C.[12] Notably, the variant G98M has a pH dependency of its activity comparable to that of the wild-type enzyme (Figure S3 in the Supporting Information). In accordance with Crismaru et al., we could determine activity of the ω-VpTA from pH 5 to 9 but none above pH 9.[36]

In summary, it was clearly demonstrated that FoldX calculations can minimize experimental effort for directed mutagenesis experiments, especially if no suitable high-throughput screening assay is available. On the other hand, it is known that FoldX libraries contain many predicted sites that even destabilize proteins or have no influence on stability.[39] To enhance the prospects of FoldX, Komor et al. performed their predictions by using a sophisticated approach to gain a consensus sequence by comparing calculations with closely related enzymes to increase the stability.[40] Using this strategy, the thermostability was increased for the fungal cellobiohydrolase I by 2.1 °C by single mutation, and the authors showed that 24% of their selected FoldX predictions were stabilizing.[41] We also found that approximately 20% of the predicted mutant proteins that we expressed resulted in stabilization. In contrast, by using only random-based approaches, the success rate tends to be approximately 2%.[41]

Our best $\Delta\Delta G$ prediction, G165M, showed a 3.3-fold reduction in enzymatic activity and an only a slight improvement in the T_m value, which stresses the importance of experimental evaluation of the theoretical data. For this specific mutation, the distance to catalytically active K267 (Scheme 1) is 13.5 Å but only 5.0 Å to Y159. Y159 is important for the coordination of the cofactor PLP at the active site and can be found in many *S*-selective ω-TAs at the same position at approximately amino-acid residue 150.[5,19,36,42] Such important sides are not automatically excluded by FoldX and have to be selected manually. Furthermore, strong discrepancy between the highly beneficial predicted $\Delta\Delta G_{Foldx}$ value and the real $\Delta\Delta G$ value (as determined by T_m) is seen for G165M and for E391K (Table 2). The low correlation of $\Delta\Delta G_{Foldx}$ to $\Delta\Delta G_{real}$ has also been observed by others and shows that FoldX can be used to predict stability trends but not to predict accurate values, as the accuracy tends to be low, especially for $\Delta\Delta G$ values, which is indicative of highly stabilizing mutations.[43–46] However, the general standard error of the FoldX algorithm is known to be only approximately 1.7 kcal mol^{-1}, which is small in comparison with the theoretical $\Delta\Delta G$ values of G165M (54.3) and E391K (42.9).[41] To improve the suggestions obtained by the FoldX algorithm further, an additional conservation analysis should be performed to avoid nonfunctional proteins by excluding highly conserved amino-acid positions.

Our best variant, G98M, is located close to the only point of symmetry of the dimer (position 92) at the end of an α helix, which is oriented parallel to the same α helix in chain B. Interface regions are very important for the stability of multimeric proteins and protein complexes and especially for the activity of ω-TA, as the active center is located at the interface region and residues of both subunits are involved.[26,47,48] These interface-interacting residues are also often hydrophobic and are, thus, involved in the stabilization of the monomer–monomer interface.[49–51] The newly introduced side chain in the case of our best variant was that of methionine, which is known to interact with oxygen atoms and also with aromatic amino acids

without the participation of protons. This can be explained by the weak dipole of Met, which makes Met an acceptor for hydrogen bonds. Met is also known for hydrophobic interaction with residues at short distances.[28] The distance of interaction with non-hydroxy oxygen atoms is often within 4.0 Å. Also well known are interactions of the sulfur atom with aromatic amino acids at a very similar distance of 3.6 Å.[52] To identify possible points of interaction of the G98M mutation and to gain insight into the structural reasons for the thermostabilization, we calculated the rotamers of M98 on the basis of the 4AOA structure and assessed the distances to the neighboring amino-acid rotamers with the highest probability in an area of 6.5 Å (Figure 5). In this range, no aromatic residue can be found, excluding stabilization through this interaction. Only oxygen-containing E94 is in a short distance of 5.8 Å, and this might lead to the formation of a hydrogen bond between E94 and M98.[52] Chain B residue R55 is at a distance of 5.7 Å. The closest neighboring amino acid would be A54 (chain B) with 3.7 Å. In addition, a hydrophobic interaction with residues around M98 (magenta colored) would be possible.

To elucidate further the molecular basis for stabilization of ω-VpTA, a molecular dynamics (MD) simulation was performed by using the structure 4AOA of the wild-type enzyme. One measure for the macromolecular flexibility and movement of amino-acid residues is the root-mean-square fluctuation (RMSF) value, which is a very sensitive parameter for comparing the distances of the atom positions during a trajectory.[54] Low RMSF values imply rigid parts of the protein, and high values denote flexible parts. According to the calculated RMSF values, G98M is positioned within the enzyme in an environment that seems to be a highly flexible (Figure S4). Also, the mutation site G165M, which was the best FoldX energy hit, is a highly flexible residue in the simulation. The use of flexible residues as targets for potential stabilizing mutations is a promising approach that has been evaluated by several groups.[39,54] According to wood-barrel theory, these residues are more important for stability than residues in rigid parts of the protein.[55] One approach to describe flexible residues is the B-factor, also known as the Debye–Waller factor; it represents the thermal motion of the atoms or residues within a protein structure and is determined by X-ray scattering of the protein crystals.[56,57] Huang et al. preselected mutation sites for enzyme stabilization guided by the B-factor as a parameter for the dynamic mobility of the parts of the enzyme and identified one single mutation with an improvement in the T_m value of 5 °C. Additionally, they selected some sites with minor improvements. The prediction success rate for the *R*-selective ω-TA from *A. terreus* was 21 %, and a control experiment without preselection was missing, but only the comparison showed if the preselection could lead to a more robust approach.[28] The B-factor of crystal structures might be an interesting indicator to detect regions within the protein with higher flexibility, but for the preselection of mutations it has to be taken into account that flexibility can also be important for the activity of an enzyme, as in the case of substrate-induced conformational changes or surface activations. In the case of the ω-TA in our study, MD calculations clearly show that the stabilizing position G98 and the neutral position G165 are both located at highly flexible parts within the amino-acid sequence. An MD simulation can predict other flexible parts that are not shown by the B-factor.[39] FoldX-predicted mutations, which were predicted to have a large energy benefit but showed only a slight or no energy benefit, can be found in areas with a low flexibility of 0.15 nm. Preselection by RMSF calculations or by comparison to *B*-factors is highly recommended and should be further investigated. For example, the FoldX-predicted mutation E391K, which showed a decrease in T_m, is even in a very rigid region with a RMSF value under 0.1 nm, which shows that FoldX predictions do not necessarily correlate with flexibility.

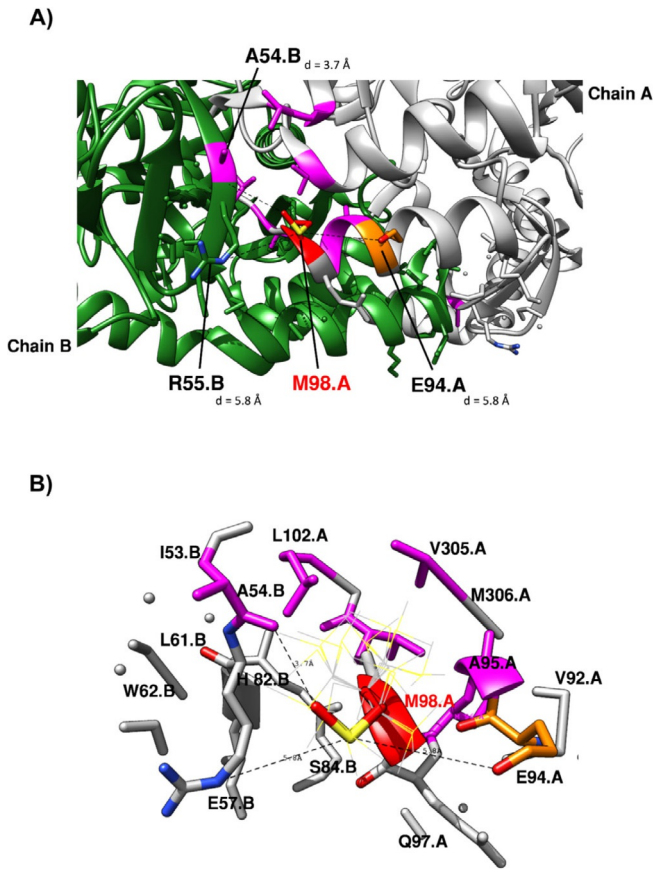

Figure 5. A) Possible interaction sites of G98M in the range of 6.5 Å. The rotamers were predicted and visualized with Chimera 1.1.[53] B) Close up of panel A: hydrophobic residues are colored magenta, and glutamate 94 is colored orange. Residues in dimers A/B are labeled with A and B.

G98M is situated in a region at the monomer–monomer interface that shows high flexibility and is at the same time a FoldX-predicted site for energy improvement. As the monomer–monomer interaction is crucial for the enzymes' activity but cannot be calculated easily, a mutation at this site might give rise to an additional benefit in the binding energy.

However, the stability improvement might also be caused by a global effect on protein flexibility, which changes the fluctuation of the whole protein. To investigate such an effect, we performed MD simulations based on the dimeric protein and compared the global flexibility of the wild-type with that of the G98M variant at 300 and 333 K (Figure S5). The simulation

showed clearly that the global flexibility of the whole protein, shown as the ΔRMSF (wild-type to G98M) value for each position, was reduced if Gly98 was exchanged to methionine. Furthermore, at 333 K the behavior of the G98M mutant remained largely unchanged relative to the simulation at 300 K, whereas the wild-type clearly showed less thermostability (Figure S5). All effects described here can contribute to the observed gain in thermostability. This demonstrates that the prediction and explanation of (de)stabilization effects is multidimensional and can be explained by using many approaches. The interactions of amino-acid residues can be explained by direct physical interactions with other residues at short distances, but changes in stability can also be derived from a global context, which cannot be predicted by using FoldX calculations.

Conclusions

In this work, a *V. paradoxus* transaminase (ω-VpTA) variant with an improved melting point of Δ4 °C was created by FoldX and site-directed mutagenesis. The FoldX-predicted improvement of 34 kcal mol^{-1} in the $\Delta\Delta G^{unfold}$ was considerably lower than the experimentally determined $\Delta\Delta G^{unfold}$ value of 15 kcal mol^{-1} for the single-site mutant G98M. This ω-VpTA variant showed activity similar to that of the wild-type enzyme but had at least a threefold increase in the half-life time at the optimum reaction temperature of 55 °C. The variant G98M can thus be used as a starting point for further random mutagenesis experiments and for screening towards new substrate specificities and as a more efficient enzyme for chiral resolution of *rac*-β-phenylalanine. In future experiments, the possibilities of more sophisticated computational approaches should be investigated to generate small, smart enzyme libraries for the generation of thermostable enzymatically active proteins. However, the data presented here and in other studies strongly stress the necessity for experimental confirmation of bioinformatic predictions.

Experimental Section

Chemicals: Unless stated otherwise, all chemicals were purchased from Sigma Aldrich and Carl Roth in analytical grade. All enantiopure β-amino acids were purchased from PepTech Corporation (Bedford, USA).

FoldX setup: To calculate the change in free energy of unfolding, the FoldX 3.0 algorithm was applied.[37] As starting point, the PDB structure 4AOA of ω-VpTA was used.[36] The in silico temperature was set to 298 K. After applying the automatic RepairPDB function, all mutations were created by using the FoldX-function BuildModel. To automate this process, a script written in Phyton was utilized to change every single amino-acid position into all standard α-amino acids possible. Other options were set to default. All resulting data for every position was ranked from lowest to highest $\Delta\Delta G$. The best nine hits showing the lowest $\Delta\Delta G$ values were chosen for mutation experiments, and in addition, two amino-acid exchanges were selected that showed a high energy benefit in terms of the FoldX energy function and a relatively high $\Delta\Delta G$ value.

Mutagenesis PCR: The mutations were generated by site-directed mutagenesis PCR by employing a touch-down PCR. Ten PCR cycles were performed by decreasing the annealing temperature by 0.5 °C each cycle, followed by 25 cycles at the calculated melting temperature of the primers. The PCR mixture was mixed according to the protocol of the Phusion DNA polymerase (Thermo Fischer Scientific), and additionally, each PCR run was performed with and without 3% (*v*/*v*) DMSO. To remove the initial DNA vector template, the endonuclease DpnI (1 μL, NEB, USA) was added to the PCR product, and the mixture was incubated for at least 1 h at 37 °C. Subsequently, the PCR product (10 μL) was transformed into 90 μL of chemical competent *E. coli* XL10 Gold (Agilent Technologies) cells. Single colonies were sequence verified by DNA sequencing of purified vector DNA (GATC, Germany).

Enzyme purification: To express the ω-VpTA in a T7 expression system, the sequence-verified plasmids were transformed into BL21 (DE3) cells. The synthetic ω-VpTA gene was ordered containing an N-terminal hexahistidine tag for purification by using immobilized metal-ion affinity chromatography. Precultures (1 mL) grown in lysogeny broth (LB) were sedimented by centrifugation in a fixed angle benchtop centrifuge (Thermo Fisher Scientific, USA) at 13 300 rpm. After washing the pellet with fresh LB, 1 mL was resuspended in 400 mL auto-inducing medium (AIM; Formedium, UK) containing 100 μg mL^{-1} ampicillin. Initially, the cultures were grown in an incubator (Infors, Switzerland) at a shaking rate of 120 rpm and 37 °C. After 4 h, the temperature was decreased to 20 °C, and the incubation was continued for 20 h. Protein expression was self-induced if D-glucose was completely consumed and the only remaining carbon source was lactose. After incubating for 24 h, the cells were collected by centrifugation at 8000 rpm in a JA-10 rotor with a Beckman Centrifuge (Coulter Beckman). The supernatant was discarded, and the cells were resuspended in lysis buffer (10 mL; 50 mM sodium phosphate, pH 7.8, 0.3 M NaCl, 10 mM imidazole, and 0.1 mM pyridoxal-5-phosphate cofactor). To lyse the cells, they were incubated with lysozyme for 30 min at room temperature and were subsequently homogenized by using ultrasonification. The cell debris was removed by centrifugation at 49 500 *g* for 30 min at 4 °C in a Beckman centrifuge. The purified ω-TA was obtained by Ni-NTA affinity chromatography with a 1 mL Ni-NTA column (Thermo Fisher) on an ÄKTA start system (GE Healthcare). To elute the ω-TA, a gradient ranging from 20 mM imidazole (lysis buffer) to 500 mM imidazole was applied at a flow rate of 1 mL min^{-1}. Fractions with ω-TA could be identified by visual inspection owing to their slight yellow color caused by bound PLP, which absorbs at λ 395 nm.[2] Fractions containing the ω-TA were pooled and concentrated by using centrifugal filters with a molecular weight cutoff of 30 kDa (Millipore). The samples used for the thermal shift assay were subjected to one freeze and thaw cycle. The purity was checked by using SDS-PAGE with 12% (*v*/*v*) acrylamide gels according to Lämmli et al. (Figure S1).[58] For determination of T_m, the buffer of the ω-TA samples was exchanged to 40 mM sodium phosphate (pH 7.2). The ω-TA samples for activity testes were mixed with 20% (*v*/*v*) glycerol and stored at 80 °C. The protein concentration was determined by using the Bradford assay with bovine serum albumin (BSA) standard samples of known protein concentration. An adapted protocol from Zor and Selinger was used, analyzing the wavelength at 450 and 595 nm.[59]

Activity test: The activities of the ω-TA samples were tested in sodium phosphate buffered solutions (pH 7.2) containing pyridoxal-5-phosphate (0.1 mM). The concentration of the substrate was set to 15 mM *rac*-β PA (amino donor) and 15 mM α-ketoglutaric

acid (amino acceptor). The standard reaction temperature was set to 40 °C, and the mixtures were preincubated prior to starting the reaction by the addition of enzyme solution (10 μL) to the reaction mixture (210 μL). If not indicated otherwise, the final concentration of the ω-TA was 2.5 μM. Samples (50 μL) were collected after 15 and 90 s, and the reaction was stopped immediately by the addition to preheated buffer solution (150 μL, 99 °C) with L-leucine (1 mM) as an internal standard. The samples were centrifuged in a benchtop centrifuge to remove all precipitates. The experiments were conducted in triplicate. To quantify the activity of the ω-TAs, one unit (U) was defined as the conversion of 1 μmol (*S*)-β-phenylalanine per minute.

HPLC analysis: Samples were analyzed by HPLC (Agilent 1200 Series, USA) with an automated precolumn derivatization protocol by using *ortho*-phthalaldehyde (according to Brucher et al.).[60] A reversed-phase C_{18} column (150×4.6 mm HyperClone 5 μm, Phenomenex Inc., Germany) was operated with a mobile phase of 55% methanol and 45% 40 mM sodium phosphate buffer (pH 6.5) at a constant flow rate of 1 mL min ^{1} at 40 °C. The elution of compounds from the column was analyzed at a wavelength of 337 nm by using a UV detector. The injection volume of the samples for the derivatization mixture was set to 0.5 μL. The derivatization mixture (7.5 μL) was injected onto the column. A calibration was performed by using defined concentrations of *rac*-β PA (Figure S2). β-PA was diluted in 40 mM sodium phosphate with L-leucine (1 mL). Optically pure *R* and *S* enantiomers from Peptech were used to calibrate the retention times (Burlington, USA).

Thermal shift assay: Determination of T_m was conducted with 5 μM solutions of freshly purified ω-TA in 40 mM sodium phosphate solution at pH 7.2. SYPRO-Orange (5000×) was used as fluorescence dye and was diluted to a working solution of 200× in buffer. The dye solution (3 μL) was added to protein solution (27 μL), and the fluorescence was recorded with a qPCR-cycler in transparent qPCR-stripes (Eppendorf, Germany). The solution was preincubated for 5 min at 20 °C in the cycler. A temperature gradient increasing the temperature by 0.5 °C per 30 s was employed until 90 °C was reached. The T_m was determined at the maximal slope of fluorescence intensity against time. Experiments were conducted in triplicate with ω-TA samples from two independent protein expressions.

Calculation of free-energy change: $\Delta\Delta G^{unfold}$ was calculated according to the equation of Christensen and Kepp.[38] To this end, the concentration of folded and unfolded protein was approximated by using the fluorescence intensity at 55 °C for the wild-type (WT) enzyme relative to that of the mutant (Mut) [Eq. (1)].

$$\Delta\Delta G \quad RT \ln\left(\frac{[\mathrm{Mut}_{\mathrm{folded}}]}{[\mathrm{WT}_{\mathrm{unfolded}}]} \times \frac{[\mathrm{WT}_{\mathrm{folded}}]}{[\mathrm{Mut}_{\mathrm{unfolded}}]}\right) \qquad (1)$$

Molecular dynamic simulations: All simulations were performed by using the GROMACS software suite (version 4.6.5). As protein structure, we used the dimer structure of the β-phenylalanine from *V. paradoxus* with a resolution of 0.228 nm.[36] To add water molecules, we used the SPC/E model, whereas the protein interacted through the AMBER03 force field.[61] The simulations were conducted in 0.9% (*w/v*) NaCl solution. The system was first energy minimized by using a conjugate gradient and was equilibrated for 2 ns in the NVT ensemble at 300/333 K and for 5 ns in the NpT ensemble at 300/333 K, whereas the pressure was set to 1 bar. During equilibration, the temperature was controlled by using a velocity-rescale thermostat (τ T 0.1 ps), and the pressure was controlled by using the Parrinello Rahman barostat (τ P 0.5 ps). Isothermal compressibility was set to 4.5×10^{5} bar ^{1}, which is the corresponding value for water.[62,63] Production runs were performed for 100 ns. The temperature was controlled by using a Nosé Hoover thermostat (τ T 1 ps), and the pressure was controlled by using the Parrinello Rahman barostat (τ P 1 ps) during the production runs. Bond lengths were constrained by using the LINCS algorithm.[63 66] Lennard Jones nonbonded interactions were evaluated by using a cutoff distance of 1.4 nm. Electrostatic interactions were evaluated by using the particle mesh Ewald method with a real space cutoff of 1.4 nm and a grid spacing of 0.12 nm. Long-range corrections to energy and pressure resulting from truncation of the Lennard Jones potential were accounted. The equations of motion were integrated by using a 2 fs time step.

To analyze structural fluctuations, we computed the root-mean-square fluctuation [Eq. (2)].

$$\mathrm{RMSF} \quad \sqrt{< \mathrm{B1}/t > \sum_{t_j}^{T} (x_i(t_j) \quad \overline{x_i})^2} \qquad (2)$$

in which T is defined as the duration of the simulation (time steps) and x_i is the coordinates of atom x_i at time t_j.

Acknowledgements

We acknowledge financial support of this project by the Helmholtz programme BioInterfaces in Technology and Medicine. The authors acknowledge the Federal Ministry of Science and Education (BMBF), Germany, for funding this project as part of the Molecular Interaction Engineering (MIE, funding code 031A095B) project. We thank Profs. Christof M. Niemeyer and Christof Syldatk for supporting our work.

Conflict of Interest

The authors declare no conflict of interest.

Keywords: amino acids · biocatalysis · enzyme engineering · thermostability · transaminases

[1] C. P. Henson, W. W. Cleland, *Biochemistry* **1964**, *3*, 338 345.
[2] K. E. Cassimjee, M. S. Humble, V. Miceli, C. G. Colomina, P. Berglund, *ACS Catal.* **2011**, *1*, 1051 1055.
[3] J. F. Kirsch, G. Eichele, G. C. Ford, M. G. Vincent, J. N. Jansonius, H. Gehr ing, P. Christen, *J. Mol. Biol.* **1984**, *174*, 497 525.
[4] A. C. Eliot, J. F. Kirsch, *Annu. Rev. Biochem.* **2004**, *73*, 383 415.
[5] G. G. Wybenga, C. G. Crismaru, D. B. Janssen, B. W. Dijkstra, *J. Biol. Chem.* **2012**, *287*, 28495 28502.
[6] D. Rudman, A. Meister, *J. Biol. Chem.* **1953**, *200*, 591 604.
[7] A. Meister, S. V. Tice, *J. Biol. Chem.* **1950**, *187*, 173 187.
[8] K. Yonaha, S. Toyama, M. Yasuda, K. Soda, *Agric. Biol. Chem.* **1977**, *41*, 1701 1706.
[9] M. Höhne, S. Schätzle, H. Jochens, K. Robins, U. T. Bornscheuer, *Nat. Chem. Biol.* **2010**, *6*, 807 813.
[10] J. Rudat, B. R. Brucher, C. Syldatk, *AMB Express* **2012**, *2*, 11.
[11] T. Pavkov Keller, G. A. Strohmeier, M. Diepold, W. Peeters, N. Smeets, M. Schürmann, K. Gruber, H. Schwab, K. Steiner, *Sci. Rep.* **2016**, *6*, 38183.
[12] S. Mathew, S. P. Nadarajan, T. Chung, H. H. Park, H. Yun, *Enzyme Microb. Technol.* **2016**, *87*, 52 60.

[13] B. A. Kern, D. Hendlin, E. Inamine, *Antimicrob. Agents Chemother.* **1980**, *17*, 679 685.
[14] M. Fuchs, J. E. Farnberger, W. Kroutil, *Eur. J. Org. Chem.* **2015**, 6965 6982.
[15] C. K. Savile, J. M. Janey, E. C. Mundorff, J. C. Moore, S. Tam, W. R. Jarvis, J. C. Colbeck, A. Krebber, F. J. Fleitz, J. Brands, P. N. Devine, G. W. Huisman, G. J. Hughes, *Science* **2010**, *329*, 305 309.
[16] K. S. Midelfort, R. Kumar, S. Han, M. J. Karmilowicz, K. McConnell, D. K. Gehlhaar, A. Mistry, J. S. Chang, M. Anderson, A. Villalobos, J. Minshull, S. Govindarajan, J. W. Wong, *Protein Eng. Des. Sel.* **2013**, *26*, 25 33.
[17] F. Guo, P. Berglund, *Green Chem.* **2017**, *19*, 333 360.
[18] S. M. Dold, C. Syldatk, J. Rudat in *Green Biocatalysis* (Ed.: R. N. Patel), Wiley, Hoboken, **2016**, pp. 715 746.
[19] I. V. Pavlidis, M. S. Weiß, M. Genz, P. Spurr, S. P. Hanlon, B. Wirz, H. Iding, U. T. Bornscheuer, *Nat. Chem.* **2016**, *8*, 1076 1082.
[20] A. R. Martin, R. DiSanto, I. Plotnikov, S. Kamat, D. Shonnard, S. Pannuri, *Biochem. Eng. J.* **2007**, *37*, 246 255.
[21] A. Nobili, F. Steffen Munsberg, H. Kohls, I. Trentin, C. Schulzke, M. Höhne, U. T. Bornscheuer, *ChemCatChem* **2015**, *7*, 757 760.
[22] M. S. Weiß, I. V. Pavlidis, P. Spurr, S. P. Hanlon, B. Wirz, H. Iding, U. T. Bornscheuer, *Org. Biomol. Chem.* **2016**, *14*, 10249 10254.
[23] F. Steffen Munsberg, C. Vickers, A. Thontowi, S. Schätzle, T. Meinhardt, M. Svedendahl, H. Land, P. Berglund, U. T. Bornscheuer, M. Höhne, *ChemCatChem* **2013**, *5*, 154 157.
[24] S. W. Han, J. Kim, H. S. Cho, J. S. Shin, *ACS Catal.* **2017**, *7*, 3752 3762.
[25] S. W. Han, E. S. Park, J. Y. Dong, J. S. Shin, *Adv. Synth. Catal.* **2015**, *357*, 1732 1740.
[26] K. Deepankumar, M. Shon, S. P. Nadarajan, G. Shin, S. Mathew, N. Ayyadurai, B. G. Kim, S. H. Choi, S. H. Lee, H. Yun, *Adv. Synth. Catal.* **2014**, *356*, 993 998.
[27] "Thermostable Omega Transaminases", A. R. M. Garcia, S. V. Kamat, S. Pannuri (Cambrex Karlskoga AB), **2010**, EP 1819825 B8.
[28] J. Huang, D. F. Xie, Y. Feng, *Biochem. Biophys. Res. Commun.* **2017**, *483*, 397 402.
[29] S. Mathew, K. Deepankumar, G. Shin, E. Y. Hong, B. G. Kim, T. Chung, H. Yun, *RSC Adv.* **2016**, *6*, 69257 69260.
[30] E. E. Ferrandi, A. Previdi, I. Bassanini, S. Riva, X. Peng, D. Monti, *Appl. Microbiol. Biotechnol.* **2017**, *101*, 4963 4979.
[31] M. C. Wani, H. L. Taylor, M. E. Wall, P. Coggon, A. T. McPhail, *J. Am. Chem. Soc.* **1971**, *93*, 2325 2327.
[32] S. G. Van Lanen, P. C. Dorrestein, S. D. Christenson, W. Liu, J. Ju, N. L. Kelleher, B. Shen, *J. Am. Chem. Soc.* **2005**, *127*, 11594 11595.
[33] Y. K. Jiang, *J. Mol. Model.* **2010**, *16*, 1239 1249.
[34] I. L. Karle, H. N. Gopi, P. Balaram, *Proc. Natl. Acad. Sci. USA* **2001**, *98*, 3716 3719.
[35] S. Parween, A. Misra, S. Ramakumar, V. S. Chauhan, *J. Mater. Chem. B* **2014**, *2*, 3096 3106.
[36] C. G. Crismaru, G. G. Wybenga, W. Szymanski, H. J. Wijma, B. Wu, S. Bartsch, S. de Wildeman, G. J. Poelarends, B. L. Feringa, B. W. Dijkstra, D. B. Janssena, *Appl. Environ. Microbiol.* **2013**, *79*, 185 195.
[37] J. Schymkowitz, J. Borg, F. Stricher, R. Nys, F. Rousseau, L. Serrano, *Nucleic Acids Res.* **2005**, *33*, W382 W388.
[38] N. J. Christensen, K. P. Kepp, *J. Chem. Inf. Model.* **2012**, *52*, 3028 3042.
[39] H. J. Wijma, R. J. Floor, P. A. Jekel, D. Baker, S. J. Marrink, D. B. Janssen, *Protein Eng. Des. Sel.* **2014**, *27*, 49 58.
[40] R. S. Komor, P. A. Romero, C. B. Xie, F. H. Arnold, *Protein Eng. Des. Sel.* **2012**, *25*, 827 833.
[41] A. Broom, Z. Jacobi, K. Trainor, E. M. Meiering, *J. Biol. Chem.* **2017**, *292*, 14349 14361.
[42] M. Genz, C. Vickers, T. van den Bergh, H. J. Joosten, M. Dörr, M. Höhne, U. T. Bornscheuer, *Int. J. Mol. Sci.* **2015**, *16*, 26953 26963.
[43] N. Tokuriki, F. Stricher, L. Serrano, D. S. Tawfik, *PLoS Comput. Biol.* **2008**, *4*, 35 37.
[44] I. E. Sánchez, J. Tejero, C. Gómez Moreno, M. Medina, L. Serrano, *J. Mol. Biol.* **2006**, *363*, 422 432.
[45] V. Frappier, M. Chartier, R. J. Najmanovich, *Nucleic Acids Res.* **2015**, *43*, W395 W400.
[46] V. Potapov, M. Cohen, G. Schreiber, *Protein Eng. Des. Sel.* **2009**, *22*, 553 560.
[47] M. S. Humble, K. E. Cassimjee, M. Häkansson, Y. R. Kimbung, B. Walse, V. Abedi, H. J. Federsel, P. Berglund, D. T. Logan, *FEBS J.* **2012**, *279*, 779 792.
[48] A. Martinez del Pozo, P. W. van Ophem, D. Ringe, G. Petsko, K. Soda, J. M. Manning, *Biochemistry* **1996**, *35*, 2112 2116.
[49] J. R. Brender, Y. Zhang, I. Vakser, E. Kellogg, J. Stephany, D. Baker, *PLOS Comput. Biol.* **2015**, *11*, e1004494.
[50] J. K. Morrow, S. Zhang, *Curr. Pharm. Des.* **2012**, *18*, 1255 12565.
[51] S. Jones, J. M. Thornton, *Prog. Biophys. Mol. Biol.* **1995**, *63*, 31 65.
[52] D. Pal, P. Chakrabarti, *J. Biomol. Struct. Dyn.* **2001**, *19*, 115 128.
[53] E. F. Pettersen, T. D. Goddard, C. C. Huang, G. S. Couch, D. M. Greenblatt, E. C. Meng, T. E. Ferrin, *J. Comput. Chem.* **2004**, *25*, 1605 1612.
[54] L. J. Smith, X. Daura, W. F. van Gunsteren, *Proteins Struct. Funct. Genet.* **2002**, *48*, 487 496.
[55] J. Chen, H. Yu, C. Liu, J. Liu, Z. Shen, *J. Biotechnol.* **2013**, *164*, 354 362.
[56] P. Debye, *Ann. Phys.* **1913**, *348*, 49 92.
[57] I. Waller, *Zeitschrift für Phys.* **1923**, *17*, 398 408.
[58] U. Lämmli, *Nature* **1979**, *277*, 680 685.
[59] T. Zor, Z. Selinger, *Anal. Biochem.* **1996**, *236*, 302 308.
[60] B. Brucher, J. Rudat, C. Syldatk, O. Vielhauer, *Chromatographia* **2010**, *71*, 1063 1067.
[61] H. J. C. Berendsen, J. R. Grigera, T. P. Straatsma, *J. Phys. Chem.* **1987**, *91*, 6269 6271.
[62] G. Bussi, D. Donadio, M. Parrinello, *J. Chem. Phys.* **2007**, *126*, 14101.
[63] M. Parrinello, A. Rahman, *J. Appl. Phys.* **1981**, *52*, 7182 7190.
[64] S. Nosé, *Mol. Phys.* **1984**, *52*, 255 268.
[65] W. G. Hoover, *Phys. Rev. A* **1985**, *31*, 1695 1697.
[66] B. Hess, H. Bekker, H. J. C. Berendsen, J. G. E. M. Fraaije, *J. Comput. Chem.* **1997**, *18*, 1463 1472.